

OPTIMIZATION FOR BRAIN ACTIVITY MONITORING WITH NEAR INFRARED LIGHT IN A FOUR-LAYERED MODEL OF THE HUMAN HEAD

Zefei Guo^{1, 2, †}, Fuhong Cai^{1, †}, and Sailing He^{1, 2, 3, *}

¹Centre for Optical and Electromagnetic Research, Zhejiang Provincial Key Laboratory for Sensing Technologies, JORCEP [Joint Research Center of Photonics of the Royal Institute of Technology, Lund University and Zhejiang University], Zijingang Campus, Zhejiang University (ZJU), Hangzhou 310058, P. R. China

²ZJU-SCNU Joint Research Center of Photonics, South China Academy of Advanced Optoelectronics, South China Normal University (SCNU), Guangzhou 510006, P. R. China

³Department of Electromagnetic Engineering, Royal Institute of Technology, Stockholm 10044, Sweden

Abstract—We describe a four-layered model for near infrared light propagation in a human head based on the Monte Carlo method. With the use of three-dimensional voxel-based media discretization, photon migration in the brain is analyzed by both the time-of-flight measurement and the spatial sensitivity profile. In the measurement of brain activity, the selection of light wavelength and the distance between the source and the detector have a great influence on the detected signal. In this study, we compare the detected signals from the detectors with different source-detector spacing at wavelengths of 690 nm, 800 nm and 1300 nm, and find that in our model, the wavelength of 1300 nm is more appropriate for the measurement of brain activity because the signals at 1300 nm get better detection sensitivity and spatial resolution. Source-detector spacing is also optimized.

Received 2 April 2013, Accepted 10 May 2013, Scheduled 4 June 2013

* Corresponding author: Sailing He (sailing@jorcep.org).

† These authors contribute equally to this study.

1. INTRODUCTION

Since near infrared spectroscopy (NIRS) was first proposed for the noninvasive monitoring of oxygen sufficiency in human brain tissue by F. F. Jobsis [1] in 1977, more and more near infrared spectroscopy and imaging models and techniques have been introduced to the area of noninvasive measurement of brain activity [2–4]. For example, E. Okada proposed several different human brain models in [2]. D. A. Boas simulated the photon migration through the human head based on a 3D Monte Carlo method [3].

In NIRS, the selection of light wavelength is clinically very important because the optical parameters of tissue vary quite much at different wavelengths, which will lead to a great influence on the detected result (the detection sensitivity and the spatial resolution). However, there have been few investigations to compare light propagation in the human head at different wavelengths.

In this study, light propagation in a three-dimensional, four-layered model of the human brain at wavelengths of 690 nm, 800 nm and 1300 nm are simulated based on the Monte Carlo method. The results are analyzed by both the backward scattering time-of-flight profile of detectors (with different source-detector spacing) and the spatial sensitivity profile. The effect of different source-detector spacing and different wavelength selection is also discussed.

Brain activity is measured by recording the backward scattering profile in this study. The change in the detected signal between different states of the brain (peaceful or active) is mainly derived from the absorption change in the grey matter in the brain [5]. When the brain becomes more active, the blood supply of brain tissue will increase, which will lead to a change in the absorption coefficient of grey matter. Then we can use the modified Beer-Lambert law to obtain the absorption change in the brain from the change of intensity and profile of the detected signal to indicate the state of the brain [6].

The distance between the source and detector also has a great influence on the detected signal in the brain activity monitoring system. If the source-detector spacing is too small, the change in the optical parameters of grey matter can not be reflected in the detected signal, meaning that the result is not sensitive to the optical parameter change of grey matter. However, if the source-detector spacing is too large, the detected signal will be very weak, leading to a low signal-to-noise ratio. Therefore, we need to find a proper source-detector spacing to measure the absorption coefficient change of the grey matter in the human brain.

2. METHOD

2.1. Human Head Model

The three-dimensional human head model used in this study is an inhomogeneous slab that consists of four different homogeneous layers [2, 7]. The geometry of the model is shown in Fig. 1. The brain tissue is segmented into five types of tissue, which include the scalp, skull, CSF (Cerebral Spinal Fluid), grey matter, and white matter. The scalp and skull are treated as one layer. Based on the three-dimensional voxel-based discretization, the brain model is gridded into $120 \times 120 \times 41$ cubic elements with side lengths of 0.1 cm. According to the layer that the element belongs to, every element is specified by its scattering coefficient and absorption coefficient. The optical properties of each layer in the human head model for the near infrared light of wavelengths of 690 nm, 800 nm and 1300 nm are shown in Table 1. There are two grey matter absorption coefficient values in Table 1, because the absorption coefficient of grey matter varies in different brain states. The first one is the absorption coefficient of grey matter when the brain is in peace while the second is that value when the brain is active. The optical properties for these layers have been chosen from the reported data on the optical properties of tissue [8–10]. Since there are no experimental results about the optical properties of grey matter and white matter at the wavelength of 1300 nm, we estimate them according to their 300–1100 nm profile in [8].

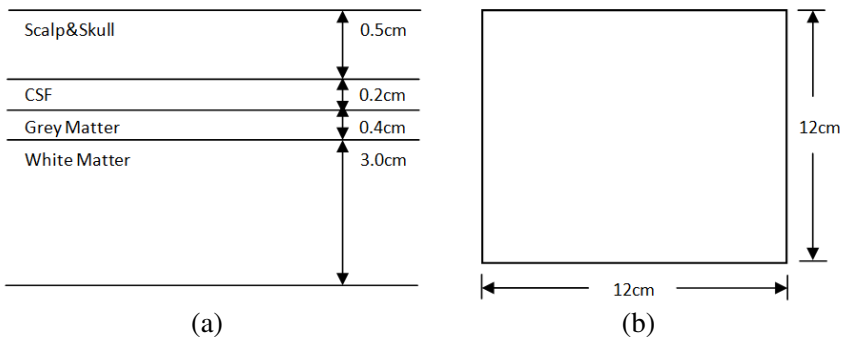


Figure 1. Schematic design for the human head model. (a) is the xz section profile and, (b) is the xy section profile of the model. The brain model consists of $120 \times 120 \times 41$ cubic elements with side lengths of 0.1 cm. Different elements get different scattering and absorption coefficient according to the layer that the element belongs to.

Table 1. Optical properties of the human head model.

Tissue Type	690 nm		800 nm		1300 nm	
	μ_s/cm^{-1}	μ_a/cm^{-1}	μ_s/cm^{-1}	μ_a/cm^{-1}	μ_s/cm^{-1}	μ_a/cm^{-1}
Scalp & Skull	94.5	0.12	86	0.1	66.5	0.6
CSF	0.10	0.02	0.09	0.04	0.01	1.0
Grey matter	100	0.18/0.30	90	0.2/0.35	66.5	0.6/1.0
White matter	365	0.9	350	1.0	100	0.6

In Table 1, μ_s and μ_a is the scattering and absorption coefficient of tissue respectively.

2.2. Monte Carlo Simulation

In many bio-photonics applications, the Monte Carlo method [11, 12] is often used to model photon migration in biological tissue. It is a very versatile method in solving numerical computing problems [13–15]. The principles of the Monte Carlo algorithm based on the variance reduction technique have already been described in [16]. The photon migration trajectory is determined by the scattering coefficient μ_s , the scattering anisotropy factor g and the random number. In this study, the anisotropy, g , is assumed to be 0.8 and the refractive index of all the layers in the brain is assumed to be 1.37. The scattering step size is corrected when the photon crosses the boundary of the elements that have different optical properties. Only when the photon is scattered out of the superficial layer of the head model will the reflection due to the refractive-index mismatch be taken into consideration. The survival weight w and total path length L of the detected photons are both recorded for each detection position. The photon weight is reduced by the Beer-Lambert law. Different wavelengths lead to different detected intensities due to the different optical properties of the human head model (see Table 1). By using Steady-State Monte Carlo simulation, at the wavelength of 690 nm, the normalized detected intensities of a peaceful brain with a source-detector spacing of 0.1 cm, 0.5 cm and 1.0 cm are 1.763×10^{-2} , 4.691×10^{-4} and 3.048×10^{-5} , respectively, while at the wavelength of 800 nm, the detected intensities of those detectors are 6.546×10^{-3} , 2.085×10^{-4} and 1.536×10^{-5} , respectively. The detected intensities at the wavelength of 1300 nm are 1.575×10^{-3} , 3.214×10^{-5} and 8.142×10^{-7} , respectively.

To find the proper source-detector spacing to measure the absorption coefficient change of the grey matter, 40 detectors with source-detector spacing from 1 mm to 40 mm are placed on the head.

The trajectories of the detected photons weighted by the detected intensity are accumulated in every element in order to get the spatial sensitivity profile.

2.3. Time-resolved Photon Migration

Here we study time-resolved photon migration using a similar approach as in [3], which has already been validated by experiments elsewhere [17]. As we have recorded the total path length L of all the detected photons, we can calculate how long time the photon has travelled in the brain before it is detected:

$$t = \frac{L}{c/n} \quad (1)$$

We set some time gates in each detection position and assign an array for each detector to record the photon weight whose propagation time matches these time gates. For every detected photon, we keep track of the elapsed time of propagation according to Equation (1) and accumulate the survival weight of the photon to the array of the matched time gate. In this study, the time gate is set from 1.827 ps to 913.333 ps.

In our simulation, we take the following 3 steps to find the proper source-detector spacing:

1. 50 billion photons are injected one by one from the source position at 690 nm and 800 nm (130 billion at 1300 nm) with the optical parameters of a peaceful brain, and the backward scattering time-of-flight profiles of different detectors are recorded;

2. 50 billion photons are injected one by one from the source position at 690 nm and 800 nm (130 billion at 1300 nm) with the optical parameters of an active brain and the backward scattering time-of-flight profiles of different detectors are recorded;

3. We compare the backward scattering time-of-flight profiles obtained from step 1 and step 2 and see whether the profiles differ. If the detector can distinguish this kind of change, then it is a proper detection position.

A proper detection position with high signal-to-noise ratio would be an ideal detection position for the measurement of brain activity.

2.4. Spatial Sensitivity in Near-infrared Spectroscopy

The spatial sensitivity profile has often been used to indicate the contribution/sensitivity of some property (e.g., attenuation) change in a particular small area to the total detected signal [18]. In this study, we use the spatial sensitivity profile to compare the different

contribution of different areas in the grey matter layer to the total detected signal.

In NIRS measurements, source and detection fibers are used. The photons are collected by the detection fiber in the following 2 steps:

1. Injected from the source to the tissue. The optical intensity distribution within the tissue $P_s(r)$ is determined by accumulating the photon weight in every voxel ($120 \times 120 \times 41$ voxels in total are used in our model). A matrix containing $120 \times 120 \times 41$ elements is assigned in the model. The accumulated photon weight in every voxel is recorded as the corresponding value in this matrix. Every time a photon crosses the boundaries of the voxels and get into another voxel, the current photon weight w is accumulated to the corresponding value of the entering voxel in this matrix. After all photons are injected, the photon intensity distribution in the tissue $P_s(r)$ is obtained based on the matrix. $P_s(r)$ is also proportional to the probability a photon emitted by the source fiber propagates to a given position r ;

2. Collected by the detection fiber (on the tissue surface) from the tissue. To get the spatial sensitivity profile, we need to obtain the collection probability distribution in the tissue first. However, it takes a long time to directly calculate the probability of collecting a photon from every position in the tissue to the detector (on the tissue surface). According to the reciprocity, we can improve the computational efficiency by the reverse Monte Carlo method [19]. By setting a source at the position of the detector, we can get the optical intensity distribution $P_{s2}(r)$ in the tissue. This, according to the reciprocity, is equal to probability $P_c(r)$ of collecting light from position r to the detection fiber, which is set at the original position on the tissue surface, i.e.,

$$P_c(r) = P_{s2}(r) \quad (2)$$

$P_s(r)$ represents the probability that a photon emitted at the source location propagates to a given position r , and $P_c(r)$ represents the probability that a photon at a given position r is collected by the detection fiber. Therefore, by multiplying $P_s(r)$ and $P_c(r)$, we can get the probability that a photon emitted at the source location propagates to the position r and then collected by the detection fiber, which is just the contribution of the element at position r to the final detected signal. Thus, we can get the spatial sensitivity distribution in the tissue by calculating the value of $P_s(r) \cdot P_c(r)$ in all the elements of the tissue.

Figure 2(a) is the schematic design of the brain activity monitoring system. The grey matter layer is the target layer of interest. We take the following 2 steps to compare the contribution/sensitivity of different areas in the grey matter layer to the total detected signal:

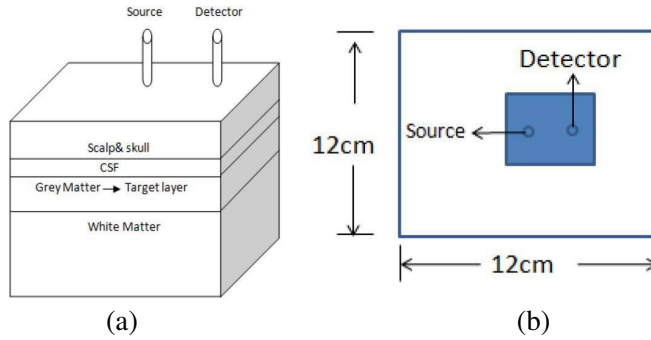


Figure 2. (a) Schematic design of the brain activity monitoring system. (b) Illustration diagram of the zone chosen to calculate the spatial sensitivity proportion of this area with respect to the whole grey matter layer. Position of the zone: x : 5.5–7.5 cm, y : 5.0–7.0 cm.

1. Record the spatial sensitivity distribution in the whole grey matter layer and get the summation of the spatial sensitivity in the whole layer as the value M_{sum} . The source is set at the position of [6.05 cm, 6.05 cm, 0] and the detector is set at [7.05 cm, 6.05 cm, 0];
 2. Get the summation of the spatial sensitivity in the zone chosen in Fig. 2(b) as the value M_{zone} ;
- With the value of M_{sum} and M_{zone} , we can assess the spatial detection resolution of this system.

3. RESULTS AND DISCUSSION

3.1. Backward Scattering Time-of-flight Profile

Simulation results of the backward scattering time-of-flight profiles for the detector 0.1 cm away from the source at wavelengths of 690 nm, 800 nm and 1300 nm are shown in Fig. 3. It compares the time-of-flight profiles in different brain states (peaceful and active). We can see that at each of the three wavelengths, the time-of-flight profiles in different brain states almost overlap. The detector cannot tell the difference between different brain states, meaning that the detected signal is not sensitive to the grey matter absorption change. Therefore, this detection position is not proper to monitor brain activity in this system. The source-detector spacing of 0.1 cm is too small at any of the three wavelengths to reflect the absorption change of grey matter.

Figure 4 directly shows the relative variation ratio of the backward time-of-flight profiles in different brain states (peaceful and active) at

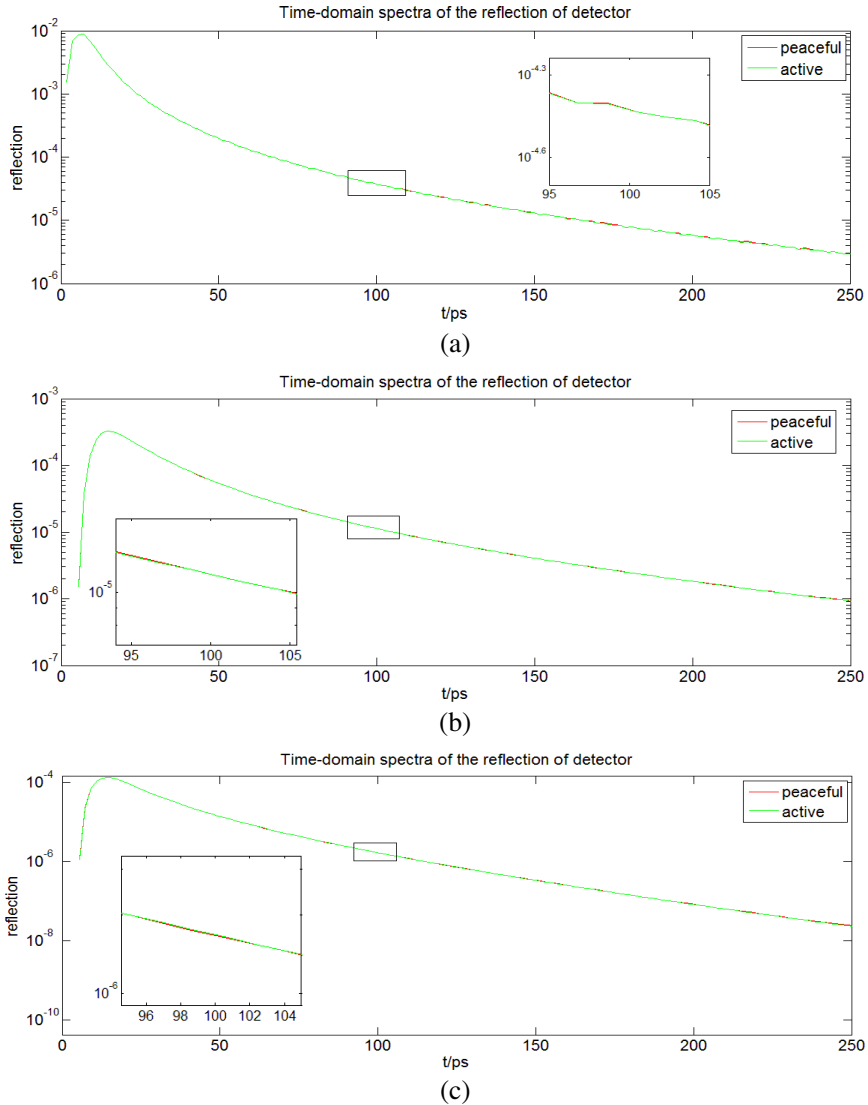


Figure 3. Backward scattering time-of-flight profile of a detector 0.1 cm from the source at the wavelength of (a) 690 nm, (b) 800 nm, and (c) 1300 nm. The red line is the profile when the brain is in peace while the green line is the profile of the active brain. The inset in (a), (b), (c) is the enlarged image of the profile in the black box zone.

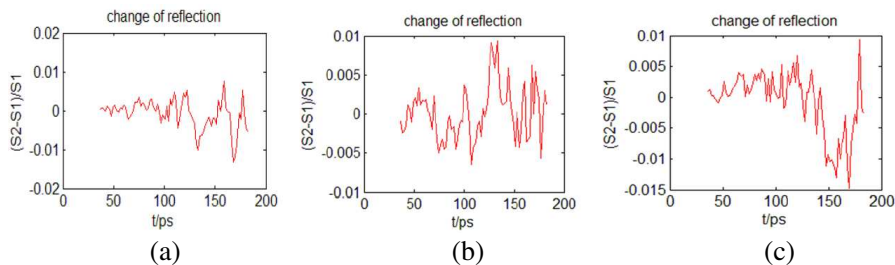


Figure 4. The relative variation ratio of the backward scattering time-of-flight profile (in different brain states) of a detector 0.1 cm from the source at the wavelength of (a) 690 nm, (b) 800 nm and (c) 1300 nm. S_1 is the backward scattering intensity in the peaceful brain. S_2 is the backward scattering intensity in the active brain. $(S_2 - S_1)/S_1$ is a dimensionless value to indicate the relative change of the response for different brain states.

a detector 0.1 cm from the source at 690 nm, 800 nm and 1300 nm. $(S_2 - S_1)/S_1$ is a dimensionless value to represent the relative variation of the backward scattering intensity in different brain states. It can be further used to indicate whether the detection position is proper for our system. With a source-detector spacing of 0.1 cm, the variation of the intensity is as small as 0.01. The fluctuation of the variation around 0 indicates that this kind of variation maybe results more from the random noise rather than the grey matter absorption change. It further proves that the source-detector spacing of 0.1 cm is too small at the three wavelengths in this system.

Figure 5 shows the results of backward scattering time-of-flight profile for a detector 0.5 cm away from the source at wavelengths of 690 nm, 800 nm and 1300 nm. It compares the profile in different brain states (peaceful and active). We can find that the profile are still smooth, and the difference of profile between different brain states is still not apparent, but can be observed after enlarged in the inset of Fig. 5 at the three wavelengths.

In Figs. 5(a) and (b), the two profile have some intersecting points in the inset indicating that the result is greatly influenced by the noise. The signal-to-noise ratio is low at 690 nm and 800 nm. The source-detector spacing of 0.5 cm is still not proper for the measurement of brain activity at the wavelength of 690 nm and 800 nm.

In Fig. 5(c), the two profiles are almost parallel without any intersection points and the profile in the active brain (green line) is lower than in the peaceful brain (red line). This conforms to our theoretical prediction. Active brain activity leads to a higher grey

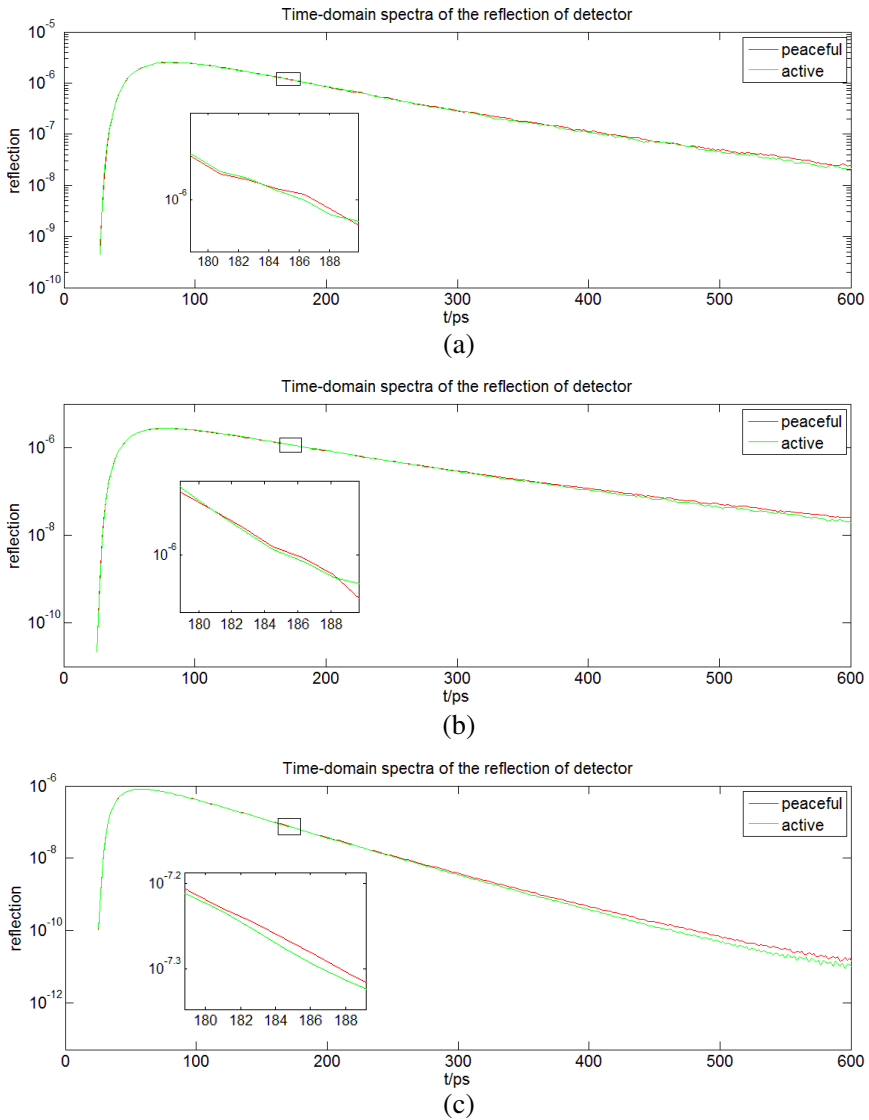


Figure 5. Backward scattering time-of-flight profile of a detector 0.5 cm from the source at the wavelength of (a) 690 nm, (b) 800 nm and (c) 1300 nm.

matter absorption coefficient [5]. According to the Beer-Lambert law, the photon weight is reduced by $\exp(-\mu_a L)$ where μ_a is the absorption coefficient and L is the total path length traveled by the

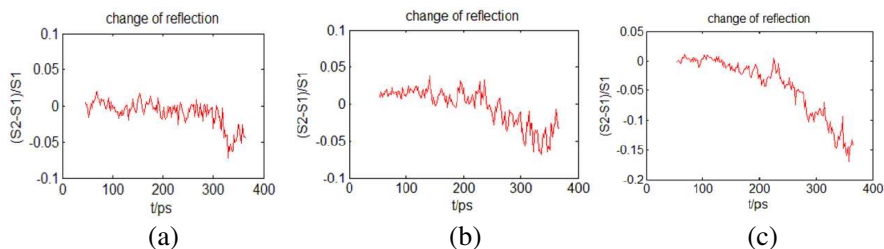


Figure 6. The relative variation ratio of the backward scattering time-of-flight profile in different brain states of a detector 0.5 cm from the source at the wavelength of (a) 690 nm, (b) 800 nm, and (c) 1300 nm.

photon. A larger absorption coefficient indicates a bigger weight loss during propagation, which will lead to a smaller detected intensity. Therefore, theoretically, the backward scattering intensity in the active brain should be smaller than in the peaceful brain without considering the influence of noise, and this is consistent with our results. The two parallel smooth profiles also indicate a high signal-to-noise ratio. Therefore, if the detector is sensitive enough to notice the difference in Fig. 5(c), this detection position with source-detector spacing of 0.5 cm will be an ideal position to monitor brain activity at the wavelength of 1300 nm.

Figure 6 directly shows the relative variation ratio of the backward scattering time-of-flight profile in different brain states (peaceful and active) of a detector 0.5 cm from the source at wavelengths of 690 nm, 800 nm and 1300 nm. It compares the relative variation between different brain states more intuitively. We find a larger relative variation at 1300 nm than 690 nm and 800 nm, indicating that the result at wavelength of 1300 nm is more sensitive to the grey matter absorption change than it at 690 nm and 800 nm. The value of the variation at 1300 nm no longer fluctuates around 0 but turns out to be always negative. In addition, the absolute value becomes larger and larger. This indicates a higher signal-to-noise ratio at 1300 nm than 690 nm and 800 nm which conforms to the conclusion drawn by Fig. 5.

Compared with a detector 0.1 cm from the source, the change in detected signal of a detector with source-detector spacing of 0.5 cm is more apparent while the profile are still very smooth. Thus, a source-detector spacing of 0.5 cm is more proper to monitor the brain activity in this system.

The results of the backward scattering time-of-flight profile for a detector 1.0 cm away from the source at the wavelength of 690 nm, 800 nm and 1300 nm are shown in Fig. 7. The difference of the profile

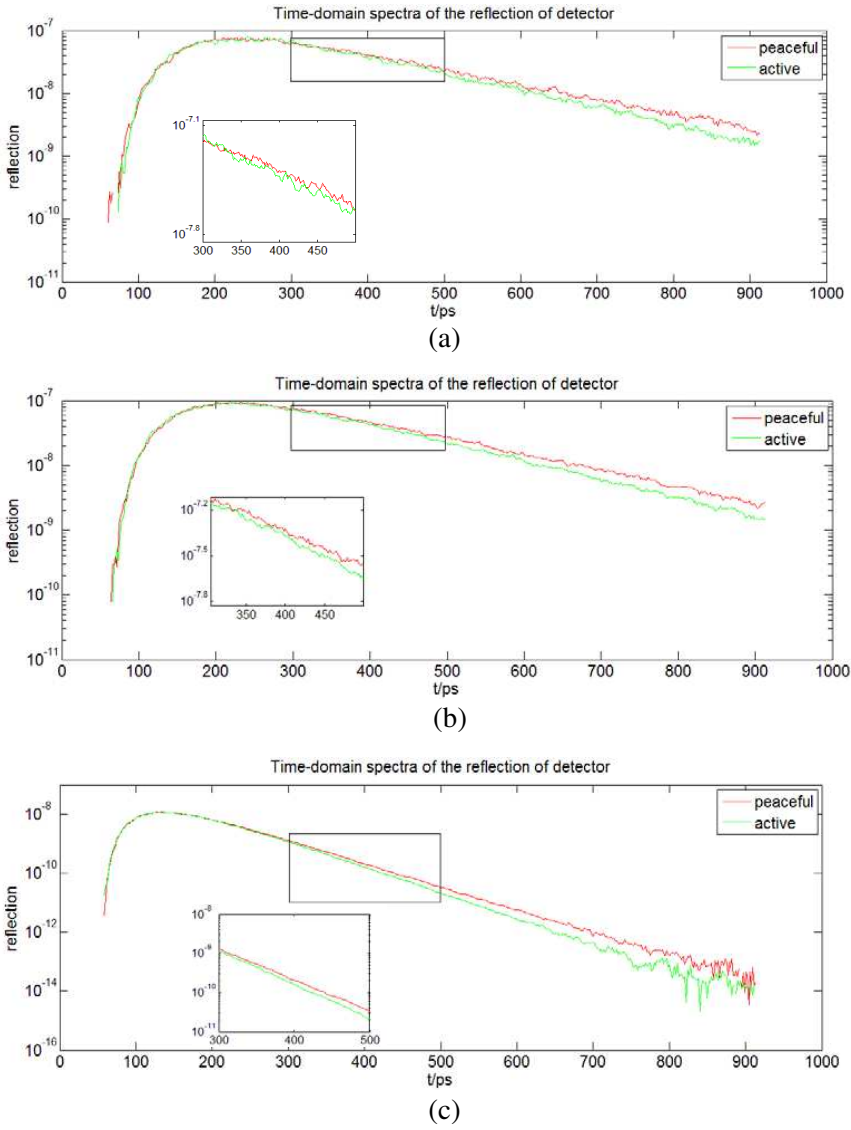


Figure 7. Backward scattering time-of-flight profile of a detector 1.0 cm from the source at the wavelength of (a) 690 nm, (b) 800 nm, and (c) 1300 nm.

between different brain states is more apparent but the profile are not as smooth as in the cases of 0.1 and 0.5 cm source-detector spacing, which indicates a greater influence from the random noise.

Figure 8 directly compares the relative variation ratio of the profile (in different brain states) of a detector 1.0 cm from the source at 690 nm, 800 nm and 1300 nm. The absolute value of relative variation is bigger at 1300 nm than 690 nm and 800 nm, indicating the profile is more sensitive to the grey matter absorption change at the wavelength of 1300 nm.

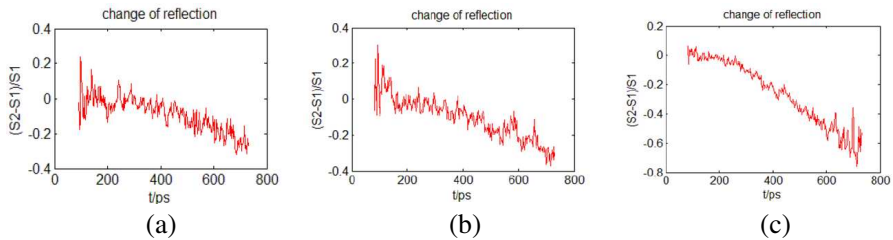


Figure 8. The relative variation ratio of the backward scattering time-of-flight profile (in different brain states) of a detector 1.0 cm from the source at the wavelength of (a) 690 nm, (b) 800 nm, and (c) 1300 nm.

Compared with a detector 0.5 cm from the source, despite improved detection sensitivity, the detected intensity gets weaker. It is necessary to take overall consideration of the two aspects when evaluating the appropriateness of this detection position.

According to the above discussions, it is found that the wavelength of 1300 nm gets better detection sensitivity than the wavelength of 690 nm and 800 nm. As we have discussed before, if the source-detector spacing is too small, we can not distinguish the grey matter absorption coefficient change by the detected signal. In this study, we found that with the same detector, we can use a smaller source-detector spacing at the wavelength of 1300 nm compared with 690 nm and 800 nm as discussed before in this section. The main drawback of the wavelength of 1300 nm in this system is its higher absorption than 690 nm and 800 nm, leading to a weaker signal. However, it can be overcome by a smaller source-detector spacing. Smaller source-detector spacing leads to stronger detected signal and better spatial resolution in this system. Therefore, we can conclude that the wavelength of 1300 nm is a better choice in this system.

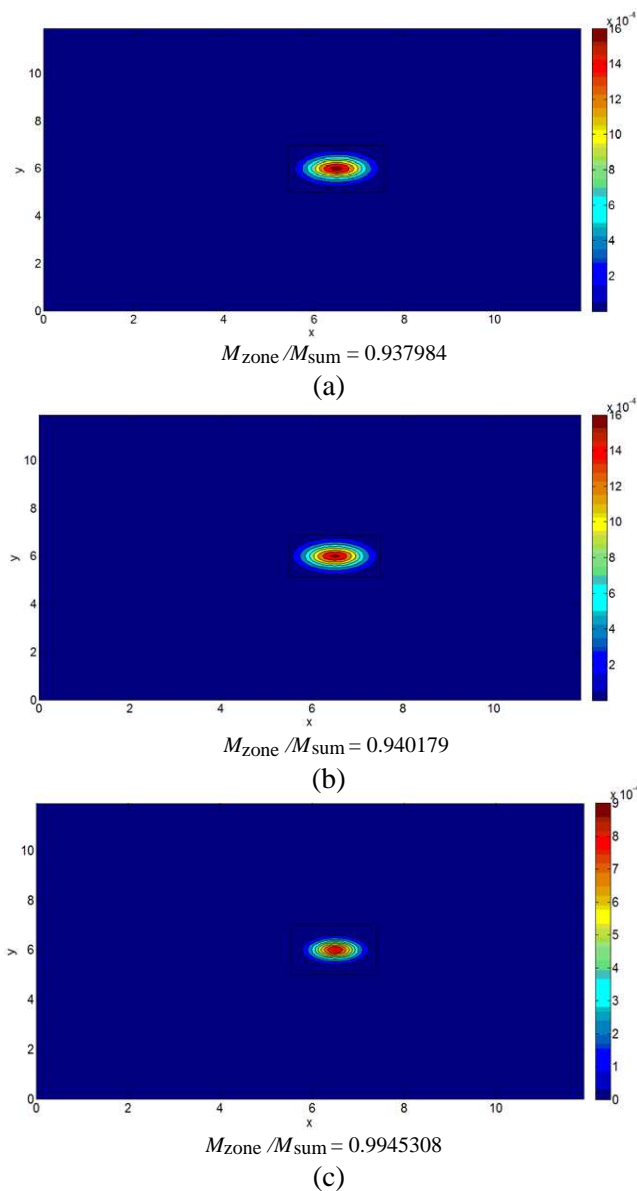


Figure 9. Spatial sensitivity profile in the grey matter layer for a source-detector of 1.0 cm at the wavelength of (a) 690 nm, (b) 800 nm, and (c) 1300 nm. M_{sum} is the summation of the spatial sensitivity in the whole layer while M_{zone} is the summation of the spatial sensitivity in the black box zone. Position of the zone: x : 5.5–7.5 cm, y : 5.0–7.0 cm.

3.2. Spatial Sensitivity Profile

Figure 9 shows the spatial sensitivity profile in the whole grey matter layer at the wavelength of 690 nm, 800 nm and 1300 nm with the system described in Section 2.4. The source-detector spacing is set to be 1.0 cm. The black box zone is the zone as shown in Fig. 2(b). It is found that the contribution to the detected signal is not homogeneous in the layer. The area between the source and detector contribute more to the final detected signal while the other areas make little contribution. The value of $M_{\text{zone}}/M_{\text{sum}}$ is the spatial sensitivity proportion of this area with respect to the whole layer. We have made similar studies with different source-detector spacing in this system.

Comparing Fig. 9(a), Fig. 9(b) with Fig. 9(c), it can be seen that the chosen 4 cm^2 area accounts for 93.8% and 94.0% contribution in the whole grey matter layer (144 cm^2) to the final detected signal at the wavelength of 690 nm and 800 nm respectively, while at the wavelength of 1300 nm, the proportion increases to 99.5%. Therefore, we can conclude that the wavelength of 1300 nm achieves better spatial precision.

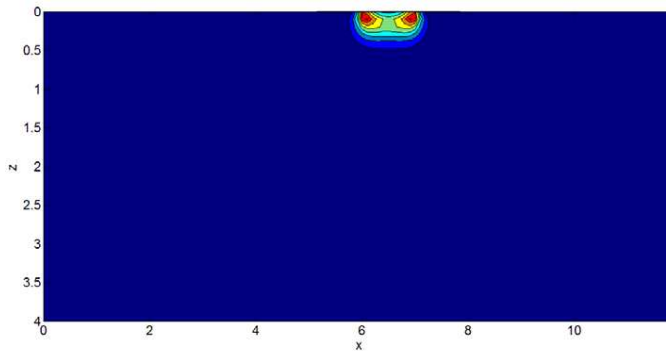


Figure 10. Spatial sensitivity profile in xz section with a detection fiber 1.0 cm from the source at the wavelength of 800 nm.

Generally speaking, imaging tissue with diffuse light (like NIRS) produces images with poor spatial resolution compared with the other imaging methods like MRI, CT and X-ray [20]. For example, the spatial resolution for non-invasive measurements of the human cortex is typically not better than 5–10 mm. With such a poor spatial resolution, it is difficult to provide enough structural details of the tissue, which are clinically very important to the diagnosis of diseases and other bio-optics applications. This is the main drawback of this kind of imaging

tools (i.e., diffuse optical tomography). To incorporate a higher spatial resolution into NIRS, it is necessary to have accurate forward models for highly heterogeneous media with arbitrary boundaries. In this study, the spatial resolution is improved in the brain activity monitoring system at the wavelength of 1300 nm. This proves that the selection of light wavelength is very important in order to get a better spatial resolution in the brain activity monitoring system and in NIRS.

Figure 10 shows the spatial sensitivity profile in xz section with a detection fiber 1.0 cm from the source at the wavelength of 800 nm and some similar result can be found in [2]. Different layers gives different contributions to the final detection signal. The layers near the superficial plane of the tissue give more contribution to the detected signal.

3.3. Experimental Feasibility Analyze

Figure 2 is the schematic design of the brain activity monitoring system. There are optical source and detectors in this system. A TCSPC system is usually used to record the time-of-flight profile in a brain activity monitoring system. To analyze the experimental feasibility, the dark noise of the PMT detector, which is usually used in TCSPC as a single-photon detector, need to be analyzed first. Some important parameters of the PMT single-photon detector are introduced in [21] and [22]. Generally speaking, the dark noise of a PMT single-photon detector is about 100 Hz (or 100 photons/s) [21].

The detected photon number (signal) of a detection fiber during one second can be calculated by

$$n_d = n \times ref \times rep \quad (3)$$

where n is the number of photons in one pulse; ref is the time-of-flight reflection at the position of the detection fiber; rep is the repetition rate of the input laser; n_d is the detected photon number per second.

A 1300 nm pulsed fiber laser was introduced in [23]. The soliton energy of the laser is 0.525 nJ, the repetition rate is 3.18 MHz, and the output optical power is 1.67 mW.

The energy of a single photon with a wavelength of 1300 nm is:

$$E = hv = h \frac{c}{\lambda} = 1.5277 \times 10^{-19} J \quad (4)$$

The number of photons in one pulse can be calculated by dividing the soliton energy by the energy of a single photon:

$$n = \frac{P_s}{P_0} = \frac{0.525 nJ}{1.5277 \times 10^{-19} J} = 3.4376 \times 10^{10} \quad (5)$$

The backward scattering time-of-flight reflection of a detector 0.5 cm away from the source at 1300 nm is between 10^{-11} and 10^{-6} as shown in Fig. 5(c). According to Equation (3), the corresponding detected photon number per second in Fig. 5(c) is between 1.0932×10^6 and 1.0932×10^{11} , which is much stronger than the dark noise of PMT. Even the reflection decreases to 10^{-14} , the signal is still one order stronger than the dark noise. Therefore, the PMT-based TCSPC is capable of recording the backward scattering time-of-flight profile in this system and is sensitive enough to distinguish the change between different brain states (active and peaceful).

In addition, a high-energy pulse laser at 1675 nm has been used in imaging the mouse brain [24], indicating that our laser is safe to be utilized in bio-imaging. The measured output soliton energy of the source is 67 nJ at a repetition rate of 1 MHz. Both the soliton energy and output power of the 1300 nm laser are much smaller than those of the 1675 nm pulse laser. Also, the absorption coefficient of water at 1300 nm (1.1 cm^{-1}) is much lower than that at 1675 nm (4.49 cm^{-1}), indicating that the optical thermal effect in 1300 nm is weaker than it in 1675 nm. Therefore, our 1300 nm laser is biologically safe and is proper for this brain activity monitoring system.

4. CONCLUSION

In this study, a four layered model of the human head has been investigated by both time-of-flight measurement and spatial sensitivity profile based on a three-dimensional Monte Carlo simulation. The difference in light propagation at the wavelength of 690 nm, 800 nm and 1300 nm has been discussed. We have found that the wavelength of 1300 nm is more appropriate for the monitoring of human brain activity. The profile is more sensitive to the grey matter absorption change at 1300 nm than 690 nm and 800 nm, and the spatial resolution is also improved at 1300 nm. The contribution to the final detected signal is not homogeneous in the grey matter layer. The area between the source and detector contributes the most to the final detected signal while the other areas have almost no effect on the detected signal.

ACKNOWLEDGMENT

This work was partially supported by the *Science* and Technology Department of Zhejiang Province (2010R50007), the National Basic Research Program (973) of China (2011CB503700), and Guangdong Innovative Research Team Program (No. 201001D0104799318).

REFERENCES

1. Jobsis, F. F., et al., "Non invasive, infrared monitoring of cerebral and myocardial oxygen sufficiency and circulatory parameters," *Science*, Vol. 198, No. 4323, 1264–1267, 1977.
2. Okada, E., et al., "Theoretical and experimental investigation of near-infrared light propagation in a model of the adult head," *Applied Optics*, Vol. 36, No. 1, 21–31, 1997.
3. Boas, D. A., J. P. Culver, J. J. Stott, and A. K. Dunn, "Three dimensional Monte Carlo code for photon migration through complex heterogeneous media including the adult human head," *Opt. Exp.*, Vol. 10, No. 3, 159–170, 2002.
4. Fukui, Y., Y. Ajichi, and E. Okada, "Monte Carlo prediction of near-infrared light propagation in realistic adult and neonatal head models," *Applied Optics*, Vol. 42, No. 16, 2881–2887, 2003.
5. Villringer, A. and B. Chance, "Non-invasive optical spectroscopy and imaging of human brain function," *Trends Neurosci*, Vol. 20, No. 10, 435–442, 1997.
6. Depty, D. T., M. Cope, et al., "Estimation of optical pathlength through tissue from direct time of flight measurement," *Phys. Med. Biol.*, Vol. 33, 1433–1442, 1988.
7. Bashkatov, A. N., E. A. Genina, et al., "Optical properties of human cranial bone in the spectral range from 800 to 2000 nm," *Proc. of SPIE*, Vol. 6163, No. 616310, 1–11, 2005.
8. Yaroslavsky, A. N., P. C. Schulze, and I. V. Yaroslavsky, "Optical properties of selected native and coagulated human brain tissues in vitro in the visible and near infrared spectral range," *Phys. Med. Biol.*, Vol. 47, 2059–2073, 2002.
9. Custo, A., W. M. Wells III, and A. H. Barnett, "Effective scattering coefficient of the cerebral spinal fluid in adult head models for diffuse optical imaging," *Applied Optics*, Vol. 45, No. 19, 4747–4755, 2006.
10. Genina, E. A., A. N. Bashkatov, and V. V. Tuchin, "Optical clearing of cranial bone," *Advanced in Optical Technologies*, Vol. 2008, No. 10, 2008.
11. Wilson, B. C. and G. Adam, "A Monte Carlo model for the absorption and flux distributions of light in tissue," *Med. Phys.*, Vol. 10, No. 6, 824–830, 1983.
12. Wang, L., S. Jaques, and L. Zheng, "MCML-Monte Carlo modeling of light transport in multi-layered tissues," *Comput. Meth. Prog. Biol.*, Vol. 47, 131–146, 1995.

13. Dai, Y., W. Liu, and X. B. Xu, "A monte carlo mpsted analysis of scattering from cylinders buried below a random periodic rough surface," *Progress In Electromagnetics Research B*, Vol. 47, 179–202, 2013.
14. Paez, E., M. A. Azpurua, C. Tremola, and R. C. Callarotti, "Uncertainty estimation in complex permittivity measurements by shielded dielectric resonator technique using the monte carlo method," *Progress In Electromagnetics Research B*, Vol. 41, 101–119, 2012.
15. Gargama, H., S. K. Chaturvedi, and A. K. Thakur, "On the Design and reliability analysis of electromagnetic absorbers using real-coded genetic algorithm and monte carlo simulation," *Progress In Electromagnetics Research B*, Vol. 43, 169–187, 2012.
16. Hiraoka, M., M. Firbank, and M. Essenpreis, "A monte carlo investigation of optical pathlength in inhomogeneous tissue and its application to near-infrared spectroscopy," *Phys. Med. Biol.*, Vol. 38, 1859–1876, 1993.
17. Fang, Q. and D. A. Boas, "Monte Carlo simulation of photon migration in 3Dturbid media accelerated by graphics processing units," *Opt. Exp.*, Vol. 17, No. 22, 20178–20190, 2009.
18. Okada, E., M. Firbank, and D. T. Depty, "The effect of overlying tissue on the spatial sensitivity profile of near-infrared spectroscopy," *Phys. Med. Biol.*, Vol. 40, 2093–2108, 1995.
19. Mcgreevy, R. L. and L. Pusztai, "Reverse Monte Carlo simulation: A new technique for the determination of disordered structures," *Molecular Simulation*, Vol. 1, 359–367, 1988.
20. Aslin, R. N. and J. Mehler, "Near-infrared spectroscopy for functional studies of brain activity in human infants: Promise, prospects, and challenges," *Journal of Biomedical Optics*, Vol. 10, No. 1, 011009, 2005.
21. Hadfield, R. H., "Single-photon detectors for optical quantum information applications," *Nature Photonics*, Vol. 3, 696–705, 2009.
22. Schmidt, F. E., "Development of a time-resolved optical tomography system for neonatal brain imaging," Ph.D. thesis, 163–164, University of London, 1999.
23. Song, Y. W., S. Y. Set, and S. Yamashita, "1300-nm pulsed fiber lasers mode-locked by purified carbon nanotubes," *IEEE Photonics Technology Letters*, Vol. 17, No. 8, 1623–1625, 2005.
24. Horton, N. G., K. Wang, and C. Xu, "In vivo three-photon microscopy of subcortical structures within an intact mouse brain," *Nature Photonics*, Vol. 7, 205–209, 2013.